1 **Two years online measurement of fine particulate nitrate in western**

2 **Yangtze River Delta: Influences of thermodynamics and N₂O₅ hydrolysis**

3 Peng Sun[1], Wei Nie[1,2,*], Xuguang Chi[1,2], Yuning Xie[1], Xin Huang[1,2], Zheng Xu[1,2], Ximeng Qi[1,2], ,

4 Zhengning Xu[1], Lei Wang[1], Tianyi Wang[1], Qi Zhang[3], and Aijun Ding[1,2,*]

6 [1]Joint International Research Laboratory of Atmospheric and Earth System Science s, and School of

7 Atmospheric Sciences, Nanjing University, Nanjing, 210023, China

8 [2]Jiangsu Provincial Collaborative Innovation Center of Climate Change, Nanjing, 210023, China

9 [3]Department of Environmental Toxicology, University of California, Davis, CA 95616, USA

10 Correspondence: Wei Nie (niewei@nju.edu.cn) and Aijun Ding (dingaj@nju.edu.cn)

11 **Abstract.**

12 Particulate nitrate contributes a large fraction of secondary aerosols. Despite

13 understanding of its important role in regional air quality and global climate, long-term

14 continuous measurements are rather limited in China. In this study, we conducted online

15 measurement of PM$_{2.5}$ nitrate for two years from March 2014 to February 2016 using

16 the Monitor for Aerosols and Gases in ambient Air (MARGA) in the western Yangtze

17 River Delta (YRD), eastern China, and investigate the main factors that influenced its

18 temporal variations and formation pathways. Compared to other sites in China, an

19 overall high concentration of particulate nitrate was observed with a mean value of 15.8

20 $\mu g\ m^{-3}$ (0.5 to 92.6 $\mu g\ m^{-3}$). Nitrate on average accounted for 32% of the total mass of

21 water-soluble ions and the proportion increased with PM loading, indicating that nitrate

22 is a major driver of haze pollution episodes in this region. Sufficient ammonia drove

23 most nitrate into the particle phase in the form of ammonium nitrate. A typical seasonal

24 cycle of nitrate was observed with the concentrations in winter on average two times

25 higher than those in summer mainly due to different meteorological conditions. In

26 summer, the diurnal variation of particulate nitrate was determined by the

27 thermodynamic equilibrium, resulting in a much lower concentration during daytime

28 despite of a considerable photochemical production. Air masses from polluted YRD

29 and biomass burning region contributed to the high nitrate concentration during summer.

30 In winter, particulate nitrate didn't reveal an evident diurnal variation. Regional

31 transport from northern China played an important role in enhancing nitrate

32 concentration. Eighteen nitrate episodes were selected to understand the processes that

33 drive the formation of high concentration of nitrate. Rapid nitrate formation was

34 observed during the pre-episode (the day before nitrate episode day) nights, and

35 dominated the increase of total water-soluble ions. Calculated nitrate from N_2O_5

36 hydrolysis was highly correlated to and accounted for 80 percent of the observed nitrate,

37 suggesting that N_2O_5 hydrolysis was a major contributor to the nitrate episodes. Our

38 results suggested that rapid formation of nitrate could be a main cause for extreme

39 aerosol pollution events in YRD during winter, and illustrated the urgent needs to

40 control the NO_x emission.

41 **1. Introduction**

42 Particulate nitrate (NO_3^-), as a major aerosol component in the atmosphere, reduces

43 atmospheric visibility (Charlson and Heintzenberg, 1995), influences human health,

44 alters radiative forcing and hence influences regional even global climate (IPCC, 2013).

45 Compared to the sulfate, nitrate has a larger scattering albedo under low RH conditions

46 that cause a stronger influence on visibility (Lei and Wuebbles, 2013). High

47 concentration of particulate nitrate had been demonstrated to be one of the major

48 reasons for the frequent occurrence of haze episodes in China (Wang and Zhang, 2009;

49 Wen et al., 2015; Wang et al., 2017). In recent decades, the Chinese government started

50 to control emissions of air pollutants with special effort on the SO_2 reduction. This

51 resulted in a remarkable decrease of ambient SO_2 and sulfate concentrations after 2006

52 (van der A et al., 2017; Wang et al., 2017). However, particulate nitrate, as well as its

53 proportion in PM, showed increasing trends due to the strong emission of nitrogen

54 oxides (NO_x) (Lei and Wuebbles, 2013; Yang et al., 2017).

55 Particulate nitrate can be formed from multiple pathways. Gas phase reaction of

56 NO_2 and OH radical is one major pathway to form nitric acid (HNO_3) (Calvert and

57 Stockwell, 1983), which subsequently reacts with ammonia (NH_3) to produce

58 ammonium nitrate (NH_4NO_3). As typical photochemical processes, these reactions

59 dominate daytime nitrate formation, and have been widely investigated in both field

60 and modelling studies (Sharma et al., 2007; Petetin et al., 2016). Heterogeneous uptake

61 of the photochemical formed nitric acid by alkali compounds, e.g. dust and sea salt

62 particles, is also a considerable pathway to form nitrate in some regions (Bian et al.,

63 2014). During nighttime, the hydrolysis of dinitrogen pentoxide (N_2O_5) is believed to

64 be the dominate pathway to form particulate nitrate. N_2O_5 is an important reactive

65 nitrogen species in the polluted troposphere (Brown and Dube., 2007; Osthoff et al.,

66 2006; Li et al., 2017; Brown et al., 2003; Brown and Stutz, 2012; Wang et al., 2016d;

67 Wang et al., 2017b) and accumulates via the reversible reaction between NO_2 and NO_3

68 radical produced from the reaction of NO_2 with O_3. Due to the rapid photolysis of NO_3

69 radical, the contribution of N_2O_5 hydrolysis to nitrate concentration during daytime of

70 sunny day is usually small. While during nighttime, N_2O_5 concentration can be up to

71 ppb level, and form nitric acid by reaction with water vapor, or particulate nitrate

72 directly by heterogeneous hydrolysis on the wet surface (Wang et al., 2017a; Wen et al.,

73 2018; Thornton et al., 2003). In China, the pollution episodes with high nitrate

74 concentrations mostly occurred in winter, during which the photochemical production

75 of nitrate should be overall weak. N_2O_5 hydrolysis thus has the potential to be the

76 crucial contributor, however there is still a lack of observational evidences.

77   Collecting particulate matter on a filter with subsequent ion chromatography

78 analysis in laboratories is the conventional method to measure the concentration of

79 particulate nitrate. The un-denuded filter pack system, which is most-widely used, can

80 suffer from both positive artifacts by absorbing gas-phase nitric acid, and negative

81 artifacts by the evaporation of ammonium nitrate (Nie et al., 2010; Pathak and Wu,

82 2009; Wang et al., 2010). A denuder system can minimize these sampling artifacts by

83 adding denuders to remove the interfering gases and back-up filters to collect the

84 evaporated vapers (John et al., 1988). However, the operation of such a denuder system

85   is extremely labor intensive and thus not widely used. In addition, the poor time-

86   resolution of filter-based measurement can limit our understanding on the formation

87   and chemical evolution of the particulate nitrate. To overcome these shortcomings,

88   several continuous and semi-continuous techniques have been developed based on an

89   online denuded-IC system (e.g. the ambient ion monitor (AIM), the gas and aerosol

90   collector ion chromatography (GAC-IC), the particle-into-liquid sample ion

91   chromatography (PILS-IC) and MARGA), as well as mass spectrometry (e.g. AMS).

92   Pathak et al. (2011) applied an AIM instrument in Beijing and Shanghai for one month

93   and found that the heterogeneous hydrolysis of N_2O_5 contributed 50%~100% of the

94   nighttime nitrate formation. Xue et al. (2013) deployed a PILS-IC system in Hong Kong

95   for less than a month and showed a more active nitrate formation during PM episode

96   than normal days. Wen et al. (2015) used a MARGA instrument in Yucheng, North

97   China during summer and emphasized the important roles of O_3 and NH_3 on nitrate

98   formation. Yang et al. (2017) carried out field observation with ACSM in Beijing for

99   half a month and pointed out the importance of aerosol nitrate in haze formation.

100 However, despite of an increasing number of studies using online techniques,

101 continuous measurements with more than one-year period are still very limited.

102   The Yangtze River Delta (YRD) located in the eastern China, with megacities

103 including Shanghai, Nanjing and Suzhou etc., has suffered from heavy particulate

104 matter pollution and photochemical pollution (Ding et al., 2013bc; Wang et al., 2016bc;

105 Wang et al., 2016a). Previous studies indicated an important role of nitrate in the

106 pollution episodes (Hua et al., 2015; Du et al., 2011; Yang et al., 2017). For example,

107 Zhang et al. (2015a) carried out an observation with ACSM in urban Nanjing during

108 summer and autumn, and found nitrate and organic aerosols dominated the PM_1

109 composition. Shi et all. (2014) used MARGA instrument in Shanghai for months and

110 found and increasing contribution of nitrate to PM_1 mass during pollution periods.

111 Wang et al. (2016b) reported temporal variation and transport of $PM_{2.5}$ water soluble

112 ions, including nitrate, in an urban site in Shanghai based on three-year continuous

113   measurement using MARGA. However, detailed investigation of the possible

114   mechanisms governing nitrate behaviors during haze pollution is still rare.

115   In this study, we present a 2-year continuous measurement of particulate nitrate

116   using MARGA at a rural site in Nanjing, a megacity in the western YRD region, with

117   the target to get a comprehensive understanding of particulate nitrate behaviors and

118   investigate the processes affecting nitrate in haze episodes. We first conducted general

119   statistical analysis of particulate nitrate and characterized seasonal variation and diurnal

120   pattern. A thermodynamic model was then applied to investigate the gas-particle

121   partition of nitrate. The influence of air masses was also investigated by conducting

122   backward Lagrangian dispersion modelling. Finally, we selected eighteen nitrate

123   episodes and investigated the main processes influencing their evolution.

124   **2.   Methodology**

125   2.1.   Sample site and instrumentation

126   The SORPES station (118°57′E, 32°07′N) was located on the top of a small hill (40 m

127   above sea level) in the Xianlin campus of Nanjing University located in the outskirts of

128   Nanjing, China. The station is an ideal receptor of air masses from the YRD with little

129   influence of local emissions and urban pollution from Nanjing. Detailed description can

130   be found in previous studies (Ding et al., 2013c; Ding et al., 2016a).

131   The measurement was conducted from March 2014 to Feb 2016. Hourly

132   concentrations of water soluble gases of HCl, HNO_3, HONO, SO_2 and NH_3, and water-

133   soluble ions in $PM_{2.5}$, including Cl^-, NO_3^-, SO_4^{2-}, NH_4^+, Na^+, K^+, Ca^{2+}, and Mg^{2+}, were

134   measured with a Monitor for Aerosols and Gases in ambient Air (MARGA, designed

135   and manufactured by Applikon Analytical B.V., the Netherlands) employed in

136   connection with a Thermo $PM_{2.5}$ cyclone inlet. The sampling system was comprised of

137   two parts: A Wet Rotating Denuder for gases and a Steam Jet Aerosol Collector for

138   aerosols, working at an air flow of 1 m^3 h^{-1} (ten Brink et al., 2007; Rumsey et al., 2014).

139   After each hour's collection, the samples were analyzed using ion chromatography. The

140   instrument was calibrated on an hourly basis using internal standard liquid (bromide

141 lithium), ensuring a stable and reliable ion chromatograph. Concentrations of all aerosol

142 ions and gases have a precision of 0.001μg m^{-3} (Xie et al., 2015). The PM$_{2.5}$ ion dataset

143 from the MARGA provided more than 15000 hourly samples over the 24 months of

144 measurements considering points where NO$_3^-$, NH$_4^+$ and SO$_4^{2-}$ were all available. Trace

145 gases (i.e., O$_3$, SO$_2$, NO$_x$, NO) and PM$_{2.5}$ mass concentrations were also measured at

146 SORPES (Ding et al., 2013c; Nie et al., 2015; Ding et al., 2016a), together with

147 meteorological data including wind speed/direction, temperature, and relative humidity.

148 2.2.   Thermodynamic constants and ISORROPIA II

149 Formation of ammonium nitrate involves an equilibrium reaction between the gas phase

150 NH$_3$ and HNO$_3$, and particle phase NH$_4$NO$_3$. The gas-to-particle partitioning is

151 temperature dependent, and the equilibrium constant can be calculated as follows (units

152 mol^{2}kg^{-2}atm^{-2}) (Sun et al., 2011; Seinfeld and Pandis, 2006):

153 $$K=k_{298}\, exp(a(298/T-1) +b[1+ln(298/T)-298/T]) \qquad (1)$$

154 $$K_{298}=3.5\times10^{16}(atm^{-2}),\ a=75.11,\ b=-13.5. \qquad (2)$$

155 ISORROPIA II (available at http://isorropia.eas.gatech.edu/) is a thermodynamic

156 model used commonly in inorganic aerosol research (Fountoukis and Nenes, 2007). To

157 analyze gas-into-particulate pathway for nitrate formation, HNO$_3$ was modeled with

158 ISORROPIA II run in forward model iteratively (Pusede et al., 2016; Fountoukis and

159 Nenes, 2007). ISORROPIA II was initialized as [NO$_3^-$+HNO$_3$]$_{total}$ = [NO$_3^-$]$_{aerosol}$.

160 Calculated HNO$_3$(g) was added back to [NO$_3^-$+HNO$_3$], while we always use

161 [NH$_4^+{}_{aerosol}$+NH$_3$(g)] as input total ammonium. ISORROPIA II was solved iteratively

162 until output NO$_3^-$ changed by < 2% by mass. The phase state was set as metastable. We

163 assume that gases and aerosol are in equilibrium, that aerosols are homogeneous and

164 internally mixed, and that unaccounted-for factors do not influence the thermodynamics

165 of system (Vayenas et al., 2005).

166 2.3.   Lagrangian Dispersion Modeling

167 To help understand the influence of air masses, backward Lagrangian particulate

168 dispersion modeling (LPDM) was carried out based on a method developed and

169 evaluated by Ding (Ding et al., 2013a). The LPDM was conducted using the Hybrid

170 Single-Particulate Lagrangian Integrated Trajectory model developed in the Air

171 Resource Laboratory (ARL) of the National Oceanic and Atmospheric Administration

172 using the ARL format Global Data Assimilation System data. The model calculates the

173 position of particulates by mean wind and a turbulence transport component after they

174 are released at the source point for a backward simulation. For each hour, 3000

175 particulates were released at 100 m altitude over the site and were traced backward for

176 a 3-day period. The hourly position of each particulate was calculated using a 3-D

177 particulate, i.e., horizontal and vertical, method. The residence time at 100 m altitude,

178 i.e., foot-print "retroplume", which represents the distribution of the surface probability

179 or residence time of the simulated air mass, was used to understand the contribution

180 from potential source regions (Ding et al., 2013ac; Shen et al., 2018).

181 2.4. Steady-state predictions

182 Based on their short lifetimes, the concentrations of the NO_3 radical and N_2O_5 can be

183 predicted by steady-state calculations due to lack of measurement data (Osthoff et al.,

184 2006). The formation and loss of N_2O_5 associated with a series of chemical reactions

185 are listed in Table 1. For the heterogeneous processes, we used 0.004 and 0.03 as the

186 uptake coefficients of the NO_3 radical and N_2O_5 (γNO_3 and γN_2O_5), respectively

187 (Aldener et al., 2006; Wen et al., 2015; Knopf et al., 2011; Brown et al., 2006). Due to

188 the lack of measurement during 2014 - 2016, the VOCs data used here was the average

189 of nighttime value that measured at SORPES station during the wintertime of 2017.

190 The corresponding rate constant can be found in Master Chemical Mechanism (MCM

191 version 3.1, http://mcm.leeds.ac.uk/MCM/). The uncertainty that caused by the limited

192 VOCs measurements and the variation of N_2O_5 uptake coefficient were estimated and

193 discussed in the supplement.

194 **3. Results and discussion**

195 3.1. Overall results

196 A MARGA was deployed to continuously measure the eight water-soluble ions (WSI)

197 of $PM_{2.5}$ and several gas-phase species from March 2014 to February 2016 with the

198 time resolution of 1-hour. Nitrate (NO_3^-), sulfate (SO_4^{2-}) and ammonium (NH_4^+) were

199 the major components with the two-year averaged concentrations of 15.8 (±13.4),15.3

200 (±10.6) and 10.4 (±7.6) µg m^{-3}, respectively. In the present study, we focused on nitrate,

201 and discussed the temporal variation and its association with physicochemical

202 processes. The concentration of $PM_{2.5}$ nitrate changed largely from 0.5 to 92.6 µg m^{-3}

203 during the measurement period, and accounted for 3% to 58% of total WSI (=45.7 +

204 30µg m^{-3}). The highest hourly nitrate concentration occurred on December 23, 2015

205 together with high concentrations of sulfate (65.5 µg m^{-3}), and ammonium (56.8 µg m$^-$

206 ^{3}). Heavy haze episode like this occurred at our site frequently during winter. To

207 understand the influence of wind on nitrate concentration, the wind rose plot is given

208 in Fig. S2. The prevailing winds at the SORPES station were from northeast and east

209 during the two-year observation period. Particulate nitrate tended to accumulate or

210 formed under stagnant condition of low wind speed. The wind from west and east can

211 lead to a higher nitrate concentration and also other aerosol components (Ding et al.,

212 2013bc; Shen et al., 2018), which may be associated with air masses from biomass

213 burning region and the city clusters of YRD.

214   To get an overall picture of nitrate distribution in developed region of costal China,

215 we reviewed results from available nitrate measurements in three most polluted regions

216 of North China Plain (NCP), YRD and Pearl River Delta (PRD), and summarized their

217 concentration, sampling sites and measurement techniques in Fig.1. The corresponding

218 data and references are listed in table S2. Measurements in summer and winter were

219 separated due to the large seasonal difference of particulate nitrate. Despite that these

220 measurements were from various measurement techniques, the results still can give us

221 some insights about the differences in spatial and temporal scales. First, particulate

222 nitrate generally showed the highest concentration in NCP and followed by YRD and

223 PRD. This was in consistence with the spatial distribution of NO_2 – a major gas

224 precursor of nitrate. Second, evident seasonal variations can be observed at all three

225   regions with much higher concentrations in winter. Third, an overall increase of

226   particulate nitrate was implied in NCP and YRD in the past decade, especially that

227   during summertime (shown in Fig.1a). Nevertheless, particulate nitrate in PRD

228   revealed an overall decreasing trend. It should be noted that the dataset cited in Fig. 1

229   were obtained from different sites with different techniques. Trends inferred from these

230   datasets could suffer from considerable uncertainty. Compared to these previous studies,

231   the nitrate concentration during summertime at SORPES station was lower than that in

232   NCP, but higher than that in YRD and PRD cities. In terms of wintertime, nitrate

233   concentration at SORPES station was slightly lower than that in NCP, comparable with

234   that in YRD, and higher than that in PRD.

235   Fig. 2 illustrates the occurrence frequency of the loading of particle matter in

236   different concentration ranges, and the changes of nitrate proportion along with the PM

237   loading. Noting that the PM loading here was indicated by the mass of total WSI. The

238   highest frequency of WSI concentrations occurred in a range of 20-40 $\mu g\ m^{-3}$, and

239   gradually decreased with the increasing of concentration. Heavy PM pollution with

240   WSI concentrations higher than 100 $\mu g\ m^{-3}$ occurred during more than 5% of the time

241   during this study. The contribution of nitrate to total WSI increased with the PM loading,

242   ranging from ~25% with WSI concentration lower than 20 $\mu g\ m^{-3}$ to ~ 40% when WSI

243   was higher than 140 $\mu g\ m^{-3}$. These results suggested that nitrate was a major driver of

244   haze episodes with high PM peaks in this region.

245   Fig. 3a shows the scatter plot of particulate nitrate and total WSI. The correlation

246   coefficient was 0.92 and nitrate accounted for 32% of the total WSI. Air temperature

247   greatly affected the contribution of nitrate to total WSI. Its proportion can be up to 58%

248   at in the temperature range of 0 °C to 5 °C and only 3% at the temperature higher than

249   30 °C, indicating an important role of thermodynamic equilibrium in nitrate

250   concentration. We further investigated the neutralization extent of sulfate and nitrate by

251   ammonium (Fig. 3b). Ammonium was overall enough to neutralize both sulfate and

252   nitrate, suggesting that the particulate nitrate mostly existed as ammonium nitrate at

253 SORPES station. This is different from the ammonia poor regions, where the uptake of

254 HNO_3 to dust/sea salt particles was found to be important to $PM_{2.5}$ nitrate (Griffith et

255 al., 2015). Seasonal difference can be observed for the molar ratio of ammonium to the

256 sum of sulfate and nitrate. In spring and early summer, a fraction of the particulate

257 nitrate is present as $Ca(NO_3)_2$ and KNO_3, which could explain the data points below the

258 regression line in Fig. 3b. In winter, considerable ammonium is existed as NH_4Cl (Hu

259 et al., 2017), resulting in the data points above the regression line.

260 3.2. Characteristics of fine particular nitrate in different seasons.

261 3.2.1. Seasonal pattern and its main causes

262 Fig. 4 shows the composite seasonal pattern of NO_x, $PM_{2.5}$ nitrate, sulfate and the

263 molar-based ratio of nitrate to sulfate during the 2-year period at SORPES station. The

264 seasonal variations of other related species and nitrate-to-$PM_{2.5}$-ratio are shown in Table

265 S3. Similar to the previous studies (Griffith et al., 2015), a typical seasonal variation

266 was observed for particulate nitrate (and its ratio to sulfate, i.e. NO_3^-/SO_4^{2-}), with a

267 maximum value of 23.7 $\mu g\ m^{-3}$ (140%) in January, and a minimum of 8.4 $\mu g\ m^{-3}$ (66%)

268 in August and September. Particulate sulfate exhibits a relatively less pronounced

269 seasonal pattern with a small peak in June. The low value of particulate nitrate during

270 summer can be generally explained by the higher temperature, higher and unstable

271 boundary layer and relative clean air masses induced by summer monsoon (Ding et al.,

272 2013c) despite of the increased photochemical formation. In opposite, the high values

273 during winter were generally due to the lower temperature, lower and stable boundary

274 layer and relative stronger continental outflow from the North China where

275 anthropogenic emission was relatively high due to heating in winter (Ding et al., 2013c).

276 Different chemical processes that affects nitrate concentrations between summer and

277 winter will be discussed later. NO_x, the major precursor, tracked the changes of

278 particulate nitrate, except for that during February and June. In addition, a secondary

279 peak of particulate nitrate can be observed during June, which can be explained as the

280 influence from agricultural burning in eastern China (Ding et al., 2013bc; Xie et al.,

281   2015; Shen et al., 2018). The concentrations of Potassium, a biomass burning tracer in

282   this region (Ding et al., 2013b; Xie et al., 2015), clearly showed a consistent peak (Fig.

283   S3) with both particulate nitrate and sulfate, as well as the discrepancy of NO_x and

284   nitrate concentrations (Ding et al., 2013b; Xie et al., 2015; Nie et al., 2015) shown in

285   Fig. 4. While in February, the nitrate concentration didn't show concurrent decrease in

286   NO_x during the Chinese Spring Festival (Ding et al., 2013c). The observations might

287   suggest that particulate nitrate is influenced by regional transport but not the local

288   emissions in February.

289   3.2.2.   Diurnal cycles during summer and winter

290   In Fig. 5, we show the averaged diurnal variations of particulate nitrate, nitrogen

291   dioxide, nitric acid, equilibrium constant (K), air temperature and RH during summer

292   and winter during the two years. Nitric acid was calculated by ISORROPIA II. In

293   summer (Fig. 5a), the fine particulate nitrate showed a typical diurnal cycle that the

294   maximum concentration occurred at 7:00 with the average concentration of 16.5 $\mu g\ m^-$

295   ^{3} and minimum value at 14:00 (7.2 $\mu g\ m^{-3}$). This summertime diurnal pattern of nitrate

296   is very similar with the findings in Shandong (Wen et al., 2015) and New York (Sun et

297   al., 2011). However, it is quite different from the findings in Hong Kong (Griffith et al.,

298   2015), where nitrate concentration peaks in the daytime in summer. Ambient

299   temperature and the development of boundary layer are the major drivers to the

300   observed diurnal variation of particulate nitrate, and high temperature and high

301   boundary layer during daytime lead to evaporation and dilution of the particulate nitrate

302   (Zhang et al., 2015a; Ding et al., 2016). Nitric acid, which accounted for 20% of the

303   total nitrate [NO_3^-+HNO_3], revealed its high concentration (around 2 ppb) in the

304   noontime (12:00-15:00). NO_2, the precursor of nitrate, showed a peak concentration of

305   18.2 ppb at 21:00, and remained at a high level during the whole night. The Equilibrium

306   constant, K, was calculated to understand the influence of gas-to-particulate partitioning

307   on the observed diurnal variation of particulate nitrate (Sun et al., 2011). As showed in

308   Fig. 5a, K showed the same diurnal pattern as particulate nitrate, suggesting the

309 thermodynamic is the major factor influencing the diurnal variation of particle nitrate

310 during summer.

311   In winter, the diurnal variation is small with a moderate peak at around 10:00 AM.

312 Compared to that in summer, K showed similar diurnal variation, but not correlated to

313 particulate nitrate, indicating factors other than the control of temperature. The

314 observed peak at late morning was probably due to downward mixing from the residual

315 layer where particulate nitrate was formed aloft during the night and brought to the

316 surface after sunrise following the breakup of the boundary layer (Baasandorj et al.,

317 2017; Young et al., 2016; Pusede et al., 2016). Direct vertical observations are needed

318 to further investigate this issue.

319   To further investigate factors influencing the nitrate behaviors other than

320 thermodynamics, ISORROPIA II was used to simulate the diurnal variation of nitrate.

321 Hourly concentrations of all species (both gas and aerosol phase species) at 00:00 were

322 used as the initial value of each specific day. Hourly data of temperature and relative

323 humidity were used as the input data to constrain the model. The ISORROPIA II model

324 was set as forward mode and metastable phase state. The calculated diurnal variations

325 are shown in Fig. 6 together with the observed results.

326   The differences between the calculation and the observation could be attributed to:

327 (1) the development of boundary layer, (2) the dry deposition of nitric acid, and (3)

328 chemical processes, which has not been considered yet in the model. As shown in Fig.

329 6a, the overall diurnal pattern of nitrate in summer is well captured by the model except

330 for 3 periods. The differences after midnight are likely caused by the effect of boundary

331 layer height and some chemical processes. Faster increase of model nitrate after 18:00

332 was attributed to lack of dry deposition of nitric acid in the model. During noontime the

333 observed nitrate concentration was expected to be lower than the calculated value

334 because of the development of boundary layer and stronger dry deposition of nitric acid

335 associated with stronger turbulence mixing, which were neglected in the model.

336 However, in contrast, the observation was considerably higher than the calculated value.

337   It indicates a strong production of nitrate via photochemical processes in summer.

338   Fig.6c shows that the difference between calculated and observed nitrate concentration

339   was in good correlation with the product of NO_2 and solar radiation, a proxy for the

340   production rate of nitric acid (Zhang et al., 2005; Young et al., 2016), further suggesting

341   that photo-oxidation of NO_2 is an important source of nitrate during summer, even

342   though the thermodynamic equilibrium is the dominate factor controlling the diurnal

343   cycle. Wen et al. (2018) also demonstrated that photochemical production of nitric acid

344   is a major contributor to daytime nitrate increase during summer in North China Plain.

345   In winter, the influence of thermodynamics on diurnal cycle is small since the relatively

346   low temperature throughout the day. The peaks in the morning may be caused by the

347   mixing down of a residual layer enriched of nitrate as mentioned above, while the

348   decline during the afternoon are supposed to be the result of dilution associated with

349   the boundary layer development.

350   3.2.3 Influence of air masses transport

351   Meteorological processes play a key role in air masses long-range transport and local

352   accumulation (Ding et al., 2013ac; Zhang et al., 2016; Ding et al, 2016b). In order to

353   investigate the influence of air masses transport on nitrate concentrations, Lagrangian

354   dispersion modeling was conducted for the sampling days with the top and bottom 25%

355   nitrate concentration in summer and winter, respectively (Ding et al., 2013a). Fig. 7

356   shows the retroplumes, i.e. footprint at an altitude of 100 m, of the selected days during

357   summer and winter, respectively. In summer, high concentrations of nitrate tended to

358   be associated with the air masses from west of Nanjing (mostly Anhui province) and

359   Yangtze River Delta (Suzhou-Shanghai city clusters and North Zhejiang province) (Fig.

360   7a). YRD is a high NO_x emission region (Fig. 1), air masses from which could bring

361   high concentration of NO_x to enhance the nitrate concentration at SORPES station.

362   Biomass burning is the possible cause of the high nitrate loading with air mass from the

363   west of Nanjing (Fig. S4). In winter, regional transport from northern China played an

364   important role in enhancing nitrate concentrations. As shown in Fig. 8c, a large part of

365   air masses for the highest 25% sampling days was from North China Plain, which has

366   the strongest NO_x emission in China (Fig. 1). It should be noted here that the longer

367   lifetime of particulate nitrate during winter might be the main cause to promote the

368   contribution of regional transport to the observed nitrate at SORPES. In contrast, the

369   lowest 25% sampling days during winter tended to be accompanied with the air mass

370   from Nanjing local and marine areas.

371   3.3.   Contribution of N_2O_5 hydrolysis to nitrate episodes

372   Similar to findings from previous studies (Zhang et al., 2015c), nitrate was found to

373   increase significantly during this study and become the largest contributor of $PM_{2.5}$

374   during the haze episodes (Fig. 2). Generally, these pollution episodes mainly occurred

375   in winter (Fig. 3a and Fig. 4), during which the photochemical production of nitric acid

376   should be weak. N_2O_5 hydrolysis was thus proposed to be a potential important

377   formation pathway. Here we investigated the nitrate episodes in detail and discussed

378   their relationship to the N_2O_5 hydrolysis during the nights before.

379   In Fig. 8, we show a typical case of nitrate episodes from 30 November to 2

380   December, 2015. Fast nitrate formation was observed, which was likely caused by

381   hydrolysis of N_2O_5. Nitrate increased significantly from 20.3 µg m^{-3} at 18:00 of 30

382   November to 63 µg m^{-3} at 6:00 of 1 December, 2015. The ratio of nitrate to $PM_{2.5}$ also

383   exhibited a large increase from 25% at 18:00 to 38% at 06:00. In contrast, other $PM_{2.5}$

384   components, e.g. sulfate and black carbon, showed only slight increases. High

385   concentration of NO_2, considerable level of O_3 and extremely low concentration of NO

386   provided a favorable condition towards forming NO_3 and N_2O_5 (Brown et al., 2003).

387   The meteorological conditions during these 12 hours were stable with low wind speed

388   and high relative humidity, which, combined with the relatively high concentration of

389   PM, would promote the hydrolysis of N_2O_5 (Riemer, 2003).

390   N_2O_5 concentrations were calculated by using the steady-state approximation

391   (Osthoff et al., 2006;Wang et al., 2014;Wen et al., 2015), and the result was shown in

392   Fig. 8. The calculated N_2O_5 exhibited a much higher concentration during the night of

393   30 November compared to the days before and after. Particulate nitrate formed from

394   N_2O_5 hydrolysis was then computed during the 12-hour period. Nitrate concentration

395   at 18:00 of 30 November, 2015 (20 µg m^{-3}) was selected as the initial value, and 31 µg

396   m^{-3} of particulate nitrate was produced in the following 12 hours, suggesting that

397   approximate 80% of increased particulate nitrate can be attributed to the hydrolysis of

398   N_2O_5 in this case.

399   To further understand the contribution of N_2O_5 hydrolysis, sampling days with

400   daily-averaged nitrate concentration exceeding the mean plus twice the standard

401   deviation were selected as the nitrate episode days. In total, 18 episode-days were

402   selected during the 2-year measurement, with 16 days in winter and the other 2 days in

403   biomass burning season. In Fig. 9, we presented the averaged diurnal pattern of

404   particulate nitrate and its related parameters on the 18 selected episode and pre-episode

405   days. For the episode days, particulate nitrate revealed a similar diurnal pattern as that

406   of the whole winter (Fig. 5). Nitrate maintained a high concentration during the whole

407   day with a small peak around 10:00 in the morning. However, for the pre-episode days,

408   a clear build-up of nitrate can be observed, especially during the nighttime from 17:00

409   of the pre-episode days to 1:00 of the episode days (as marked in Fig. 9). The average

410   increment of ammonium nitrate exceeded 24 µg m^{-3} during this 9-hour period of the

411   pre-episode nighttime. The total WIS also increased during this period, which was

412   mostly attributed to ammonium nitrate (almost 90%) and resulted in an evident increase

413   of the ratio of nitrate to total WSI. Compared to nitrate, black carbon, a tracer of primary

414   emissions, showed little change during the pre-episode day. The retroplume showed in

415   Fig. S5 suggested that the air masses arrived at the SORPES station on the pre-episode

416   and episode days were almost the same. These results suggest that secondary formation

417   other than accumulation was the major contributor to the observed increase of

418   particulate nitrate.

419   Since the observed nitrate formation mostly occurred during the nighttime of pre-

420   episode days when the photochemical production of nitric acid would be largely

421   suppressed, N_2O_5 hydrolysis is thus believed to be the major contributor. As showed in

422   Fig. 9, compared to those during episode days, NO_2 concentration was comparable with

423   the average concentrations of 28 ppb, the but O_3 concentration was higher during pre-

424   episode days. This resulted in a higher production rate of N_2O_5 proxy (PNO_3) in pre-

425   episode days, and favored formation of nitrate from the hydrolysis of N_2O_5. We further

426   calculated the contribution of N_2O_5 hydrolysis to nitrate formation during the periods

427   from 17:00 to 23:00 of each pre-episode day (excluding 2 windy days). A good

428   correlation (R=0.8) was observed between the calculated nitrate and observed nitrate

429   (Fig. 10), with the slope of 0.77, indicating the observed nitrate formation during nitrate

430   episodes were significantly attributed to the hydrolysis of N_2O_5. It should be noted that

431   this calculation suffered from considerable uncertainties due to the variability of actual

432   VOCs concentrations and N_2O_5 uptake coefficient. The detailed uncertainty calculation

433   is discussed in the supplement (Fig. S1).

434   **4.   Summary and Conclusion**

435   Online measurements of fine particulate nitrate along with trace gases and $PM_{2.5}$ mass

436   concentrations were conducted for two years from March 2014 to February 2016 using

437   a MARGA at SORPES station, a rural receptor site in the Yangtze River Delta, eastern

438   China. Hourly nitrate concentration varied from 0.5 $\mu g\ m^{-3}$ to 92.6 $\mu g\ m^{-3}$, with an

439   averaged value of 15.8 $\mu g\ m^{-3}$, which was generally higher than the measurement at the

440   sites in YRD and PRD, but lower than that at the sites in North China Plain. The

441   contribution of nitrate to total WSI increased from 25% with WSI concentration lower

442   than 20 $\mu g\ m^{-3}$, to 40% when WSI was higher than 140 $\mu g\ m^{-3}$, suggesting a major

443   driver of nitrate to the aerosol pollution in YRD. NH_3 is enough to neutralize the acidic

444   compounds of aerosol, and ammonium nitrate was thus the predominate form of the

445   observed particulate nitrate.   A clear seasonal variation of nitrate was observed with

446   peak value in January and December and lowest value in August and September.

447   Biomass burning plumes contributed to the nitrate concentration evidently and resulted

448   in a secondary peak during June. In summer, thermodynamic equilibrium was the major

factor influencing the diurnal variation of nitrate, and resulted in a much lower concentration at noontime. Nevertheless, the observed nitrate at noontime was considerably higher than the value predicted by the ISORROPIA II model, indicating a strong production of nitrate by the photo-oxidation of NO_2. Air masses from YRD and the biomass burning region were associated with the high nitrate concentrations during summer. In winter, the diurnal variation of nitrate was weak. Regional transport from the North China Plain contributed largely to the observed high nitrate concentrations.

Nitrate episodes, defined as daily-averaged concentration exceeding the mean value plus twice the standard deviation, were further investigated to understand the chemical processes towards forming particulate nitrate and their contribution to the pollution episodes. A clear build-up of nitrate can be observed during the pre-episode night, which dominated the increase of total WSI. N_2O_5 hydrolysis was demonstrated to contribute 80% of the observed nitrate formation, suggesting its critical role in an aerosol pollution episode. In view of the significant emission of NO, which is the main sink of N_2O_5 during night, stronger production of N_2O_5 is expected at the upper boundary layer, e.g. residual layer, and this residual layer N_2O_5 will contribute to the nitrate formation in the entire boundary layer. In summary, our study provides evidence that particulate nitrate especially that formed from N_2O_5 hydrolysis is a crucial contributor to the aerosol pollution episodes in eastern China.

Data availability. The GDAS data used in the HYSPLIT calculation can be acquired from ftp://arlftp.arlhq.noaa.gov/pub/archives/gdas1. Measurement data at SORPES, including aerosol data and relevant trace gases as well as meteorological data, are available upon request from the corresponding author before the SORPES database is opened publicly.

Acknowledgements. The research was supported by National Key Research & Development Program of China (2016YFC0200500) and National Science Foundation

475 of China (41725020, 91544231, 91644218, 41422504, 91744311, 41675145).

References

477 Aldener, M., Brown, S. S., Stark, H., Williams, E. J., Lerner, B. M., Kuster, W. C., Goldan, P. D., Quinn,
478   P. K., Bates, T. S., Fehsenfeld, F. C., and Ravishankara, A. R.: Reactivity and loss mechanisms of
479   NO3 and N2O5 in a polluted marine environment: Results from in situ measurements during New
480   England Air Quality Study 2002, J Geophys Res-Atmos, 111, 2006.

481 Baasandorj, M., Hoch, S. W., Bares, R., Lin, J. C., Brown, S. S., Millet, D. B., Martin, R., Kelly, K.,
482   Zarzana, K. J., Whiteman, C. D., Dube, W. P., Tonnesen, G., Jaramillo, I. C., and Sohl, J.: Coupling
483   between Chemical and Meteorological Processes under Persistent Cold-Air Pool Conditions:
484   Evolution of Wintertime PM2.5 Pollution Events and N2O5 Observations in Utah's Salt Lake Valley,
485   Environ Sci Technol, 51, 5941-5950, 10.1021/acs.est.6b06603, 2017.

486 Bian, Q., Huang, X. H. H., and Yu, J. Z.: One-year observations of size distribution characteristics of
487   major aerosol constituents at a coastal receptor site in Hong Kong – Part 1: Inorganic ions
488   and oxalate, Atmospheric Chemistry and Physics, 14, 9013-9027, 10.5194/acp-14-9013-2014, 2014.

489 Brown, S. S., Stark, H., Ryerson, T. B., Williams, E. J., Nicks, D. K., Trainer, M., Fehsenfeld, F. C., and
490   Ravishankara, A. R.: Nitrogen oxides in the nocturnal boundary layer: Simultaneous in situ
491   measurements of NO3, N2O5, NO2, NO, and O-3, J Geophys Res-Atmos, 108, 2003.

492 Brown, S. S., Ryerson, T. B., Wollny, A. G., Brock, C. A., Peltier, R., Sullivan, A. P., Weber, R. J., Dube,
493   W. P., Trainer, M., Meagher, J. F., Fehsenfeld, F. C., and Ravishankara, A. R.: Variability in nocturnal
494   nitrogen oxide processing and its role in regional air quality, Science, 311, 67-70, 2006.

495 Brown, S. S., and W.P.Dube.: High resolution vertical distributions of NO_3 and N_2O_5 through the
496   nocturnal boundary layer, Atmospheric Chemistry and Physics, 7, 139-149, 2007.

497 Brown, S. S., and Stutz, J.: Nighttime radical observations and chemistry, Chem Soc Rev, 41, 6405-6447,
498   2012.

499 Brown, S. S., Dube, W. P., Tham, Y. J., Zha, Q. Z., Xue, L. K., Poon, S., Wang, Z., Blake, D. R., Tsui,
500   W., Parrish, D. D., and Wang, T.: Nighttime chemistry at a high altitude site above Hong Kong, J
501   Geophys Res-Atmos, 121, 2457-2475, 10.1002/2015JD024566, 2016.

502 Calvert, J. G., and Stockwell, W. R.: Acidic generation in the troposphere by gas phase chemistry,
503   Environ. Sci. Technol., 17, 428-443, 1983.

504 Cao, J.-J., Shen, Z.-X., Chow, J. C., Watson, J. G., Lee, S.-C., Tie, X.-X., Ho, K.-F., Wang, G.-H., and
505   Han, Y.-M.: Winter and Summer PM2.5 Chemical Compositions in Fourteen Chinese Cities, Journal
506   of the Air & Waste Management Association, 62, 1214-1226, 10.1080/10962247.2012.701193,
507   2012.

508 Charlson, R., and Heintzenberg, J.: Aerosol Forcing of Climate Environmental Sciences Research Report,
509   1995.

510   Ding, A., Wang, T., and Fu, C.: Transport characteristics and origins of carbon monoxide and ozone in
511   Hong Kong, South China, Journal of Geophysical Research: Atmospheres, 118, 9475-9488,
512   10.1002/jgrd.50714, 2013a.

513   Ding, A. J., Fu, C. B., Yang, X. Q., Sun, J. N., Petäjä, T., Kerminen, V. M., Wang, T., Xie, Y., Herrmann,
514   E., Zheng, L. F., Nie, W., Liu, Q., Wei, X. L., and Kulmala, M.: Intense atmospheric pollution
515   modifies weather: a case of mixed biomass burning with fossil fuel combustion pollution in eastern
516   China, Atmospheric Chemistry and Physics, 13, 10545-10554, 10.5194/acp-13-10545-2013, 2013b.

517   Ding, A. J., Fu, C. B., Yang, X. Q., Sun, J. N., Zheng, L. F., Xie, Y. N., Herrmann, E., Nie, W., Petäjä, T.,
518   Kerminen, V. M., and Kulmala, M.: Ozone and fine particle in the western Yangtze River Delta: an
519   overview of 1 yr data at the SORPES station, Atmospheric Chemistry and Physics, 13, 5813-5830,
520   10.5194/acp-13-5813-2013, 2013c.

521   Ding, A.J., Nie, W., Huang, X., Chi, X., Sun, J., Kerminen,V.-M., Xu, Z., Guo, W., Petäjä, T., Yang, X.,
522   Kulmala, M., and Fu, C.: Long-term observation of air pollution-weather/climate interactions at the
523   SORPES station: a review and outlook, Front. Environ. Sci. & Eng., 10, 5, 15, 2016a.

524   Ding, A.J., Huang, X., Nie, W., Sun, J.N., Kerminen, V.-M., Petaja, T., Su, H., Cheng, Y.F., Yang, X.-Q.,
525   Wang, M.H., Chi, X.G., Wang, J.P., Virkkula, A., Guo, W.D., Yuan, J., Wang, S.Y., Zhang, R.J., Wu,
526   Y.F., Song, Y., Zhu, T., Zilitinkevich, S., Kulmala, M., and Fu, C.B.: Ehanced haze pollution by
527   black carbon in megacities in China, Geophys. Res. Lett., 43, 6, 2873-2879, 2016b.

528   Du, H., Kong, L., Cheng, T., Chen, J., Du, J., Li, L., Xia, X., Leng, C., and Huang, G.: Insights into
529   summertime haze pollution events over Shanghai based on online water-soluble ionic composition
530   of aerosols, Atmospheric Environment, 45, 5131-5137, 10.1016/j.atmosenv.2011.06.027, 2011.

531   Fountoukis, C., and Nenes, A.: ISORROPIA II: a computationally efficient thermodynamic equilibrium
532   model for K+-Ca2+-Mg2+-Nh(4)(+)-Na+-SO42--NO3--Cl--H2O aerosols, Atmospheric Chemistry
533   and Physics, 7, 4639-4659, 2007.

534   Gao, X. M., Yang, L. X., Cheng, S. H., Gao, R., Zhou, Y., Xue, L. K., Shou, Y. P., Wang, J., Wang, X. F.,
535   Nie, W., Xu, P. J., and Wang, W. X.: Semi-continuous measurement of water-soluble ions in PM2.5
536   in Jinan, China: Temporal variations and source apportionments, Atmospheric Environment, 45,
537   6048-6056, 2011.

538   Griffith, S. M., Huang, X. H. H., Louie, P. K. K., and Yu, J. Z.: Characterizing the thermodynamic and
539   chemical composition factors controlling PM2.5 nitrate: Insights gained from two years of online
540   measurements in Hong Kong, Atmospheric Environment, 122, 864-875,
541   10.1016/j.atmosenv.2015.02.009, 2015.

542   He, L.-Y., Huang, X.-F., Xue, L., Hu, M., Lin, Y., Zheng, J., Zhang, R., and Zhang, Y.-H.: Submicron
543   aerosol analysis and organic source apportionment in an urban atmosphere in Pearl River Delta of
544   China using high-resolution aerosol mass spectrometry, Journal of Geophysical Research, 116,
545   10.1029/2010jd014566, 2011.

546   Hu, W., Hu, M., Hu, W.-W., Zheng, J., Chen, C., Wu, Y., and Guo, S.: Seasonal variations in high time-

547   resolved chemical compositions, sources, and evolution of atmospheric submicron aerosols in the
548   megacity Beijing, Atmospheric Chemistry and Physics, 17, 9979-10000, 10.5194/acp-17-9979-
549   2017, 2017.

550   Hua, Y., Cheng, Z., Wang, S., Jiang, J., Chen, D., Cai, S., Fu, X., Fu, Q., Chen, C., Xu, B., and Yu, J.:
551   Characteristics and source apportionment of PM2.5 during a fall heavy haze episode in the Yangtze
552   River Delta of China, Atmospheric Environment, 123, 380-391, 10.1016/j.atmosenv.2015.03.046,
553   2015.

554   John, W., Wall, S. M., and Ondo, J. L.: A New Method for Nitric-Acid and Nitrate Aerosol Measurement
555   Using the Dichotomous Sampler, Atmospheric Environment, 22, 1627-1635, 1988.

556   Knopf, D. A., Forrester, S. M., and Slade, J. H.: Heterogeneous oxidation kinetics of organic biomass
557   burning aerosol surrogates by O-3, NO2, N2O5, and NO3, Phys Chem Chem Phys, 13, 21050-
558   21062, 2011

559   Lei, H., and Wuebbles, D. J.: Chemical competition in nitrate and sulfate formations and its effect on air
560   quality, Atmospheric Environment, 80, 472-477, 10.1016/j.atmosenv.2013.08.036, 2013.

561   Li, H., Zhang, Q., Zhang, Q., Chen, C., Wang, L., Wei, Z., Zhou, S., Parworth, C., Zheng, B., Canonaco,
562   F., Prévôt, A. S. H., Chen, P., Zhang, H., Wallington, T. J., and He, K.: Wintertime aerosol chemistry
563   and haze evolution in an extremely polluted city of the North China Plain: significant contribution
564   from coal and biomass combustion, Atmospheric Chemistry and Physics, 17, 4751-4768,
565   10.5194/acp-17-4751-2017, 2017.

566   Nie, W., Wang, T., Gao, X., Pathak, R. K., Wang, X., Gao, R., Zhang, Q., Yang, L., and Wang, W.:
567   Comparison among filter-based, impactor-based and continuous techniques for measuring
568   atmospheric fine sulfate and nitrate, Atmospheric Environment, 44, 4396-4403,
569   10.1016/j.atmosenv.2010.07.047, 2010.

570   Nie, W., Ding, A. J., Xie, Y. N., Xu, Z., Mao, H., Kerminen, V. M., Zheng, L. F., Qi, X. M., Huang, X.,
571   Yang, X. Q., Sun, J. N., Herrmann, E., Petäjä, T., Kulmala, M., and Fu, C. B.: Influence of biomass
572   burning plumes on HONO chemistry in eastern China, Atmospheric Chemistry and Physics, 15,
573   1147-1159, 10.5194/acp-15-1147-2015, 2015.

574   Osthoff, H. D., Sommariva, R., Baynard, T., Pettersson, A., Williams, E. J., Lerner, B. M., Roberts, J. M.,
575   Stark, H., Goldan, P. D., Kuster, W. C., Bates, T. S., Coffman, D., Ravishankara, A. R., and Brown,
576   S. S.: Observation of daytime N2O5 in the marine boundary layer during New England Air Quality
577   Study-Intercontinental Transport and Chemical Transformation 2004, Journal of Geophysical
578   Research: Atmospheres, 111, n/a-n/a, 10.1029/2006jd007593, 2006.

579   Pathak, R. K., and W.S.Wu: Summertime PM2.5 ionic species in four major cities of China; nitrate
580   formation in an ammonia-deficient atmosphere, Atmospheric Chemistry and Physics, 9, 1711-1722,
581   2009.

582   Pathak, R. K., Wang, T., and Wu, W. S.: Nighttime enhancement of PM2.5 nitrate in ammonia-poor
583   atmospheric conditions in Beijing and Shanghai: Plausible contributions of heterogeneous

hydrolysis of N2O5 and HNO3 partitioning, Atmospheric Environment, 45, 1183-1191, 10.1016/j.atmosenv.2010.09.003, 2011.

Petetin, H., Sciare, J., Bressi, M., Gros, V., Rosso, A., Sanchez, O., Sarda-Estève, R., Petit, J.-E., and Beekmann, M.: Assessing the ammonium nitrate formation regime in the Paris megacity and its representation in the CHIMERE model, Atmospheric Chemistry and Physics, 16, 10419-10440, 10.5194/acp-16-10419-2016, 2016.

Pusede, S. E., Duffey, K. C., Shusterman, A. A., Saleh, A., Laughner, J. L., Wooldridge, P. J., Zhang, Q., Parworth, C. L., Kim, H., Capps, S. L., Valin, L. C., Cappa, C. D., Fried, A., Walega, J., Nowak, J. B., Weinheimer, A. J., Hoff, R. M., Berkoff, T. A., Beyersdorf, A. J., Olson, J., Crawford, J. H., and Cohen, R. C.: On the effectiveness of nitrogen oxide reductions as a control over ammonium nitrate aerosol, Atmospheric Chemistry and Physics, 16, 2575-2596, 10.5194/acp-16-2575-2016, 2016.

Riemer, N.: Impact of the heterogeneous hydrolysis of N2O5on chemistry and nitrate aerosol formation in the lower troposphere under photosmog conditions, Journal of Geophysical Research, 108, 10.1029/2002jd002436, 2003.

Rumsey, I. C., Cowen, K. A., Walker, J. T., Kelly, T. J., Hanft, E. A., Mishoe, K., Rogers, C., Proost, R., Beachley, G. M., Lear, G., Frelink, T., and Otjes, R. P.: An assessment of the performance of the Monitor for AeRosols and GAses in ambient air (MARGA): a semi-continuous method for soluble compounds, Atmospheric Chemistry and Physics, 14, 5639-5658, 10.5194/acp-14-5639-2014, 2014.

Seinfeld, J. H., and Pandis, S. N.: Atmospheric Chemistry and Physics: From Air Pollution to Climate Change, John Wiley & Sons, New York, 2nd edition, 1232 pp., 13: 978-0-471-72018-8 2006.

Sharma, M., Kishore, S., Tripathi, S. N., and Behera, S. N.: Role of atmospheric ammonia in the formation of inorganic secondary particulate matter: A study at Kanpur, India, Journal of Atmospheric Chemistry, 58, 1-17, 10.1007/s10874-007-9074-x, 2007.

Shen, Y., Virkkula, A., Ding, A., Wang, J., Chi, X., Nie W., Qi, X., Huang, X., Liu Q., Zheng, L., Xu, Z., Petaja, T., Aalto, P.P., Fu, C. and Kulmala, M.: Aerosol optical properties at SORPES in Nanjing, East China, Atmos. Chem. Phys., 18, 5265-5292, 2018.

Shi, Y., Chen, J., Hu, D., Wang, L., Yang, X., and Wang, X.: Airborne submicron particulate (PM1) pollution in Shanghai, China: chemical variability, formation/dissociation of associated semi-volatile components and the impacts on visibility, The Science of the total environment, 473-474, 199-206, 10.1016/j.scitotenv.2013.12.024, 2014.

Sun, Y. L., Zhang, Q., Schwab, J. J., Demerjian, K. L., Chen, W. N., Bae, M. S., Hung, H. M., Hogrefe, O., Frank, B., Rattigan, O. V., and Lin, Y. C.: Characterization of the sources and processes of organic and inorganic aerosols in New York city with a high-resolution time-of-flight aerosol mass apectrometer, Atmospheric Chemistry and Physics, 11, 1581-1602, 10.5194/acp-11-1581-2011, 2011.

ten Brink, H., Otjes, R., Jongejan, P., and Slanina, S.: An instrument for semi-continuous monitoring of the size-distribution of nitrate, ammonium, sulphate and chloride in aerosol, Atmospheric

Environment, 41, 2768-2779, 10.1016/j.atmosenv.2006.11.041, 2007.

Thornton, J. A., Braban, C. F., and Abbatt, J. P. D.: N2O5 hydrolysis on sub-micron organic aerosols: the effect of relative humidity, particle phase, and particle size, Phys Chem Chem Phys, 5, 4593-4603, 2003

van der A, R. J., Mijling, B., Ding, J., Koukouli, M. E., Liu, F., Li, Q., Mao, H., and Theys, N.: Cleaning up the air: effectiveness of air quality policy for SO2 and NOx emissions in China, Atmospheric Chemistry and Physics, 17, 1775-1789, 10.5194/acp-17-1775-2017, 2017.

Vayenas, D. V., Takahama, S., Davidson, C. I., and Pandis, S. N.: Simulation of the thermodynamics and removal processes in the sulfate-ammonia-nitric acid system during winter: Implications for PM2.5 control strategies, J Geophys Res-Atmos, 110, 2005.

Wang, D., Zhou, B., Fu, Q., Zhao, Q., Zhang, Q., Chen, J., Yang, X., Duan, Y., and Li, J.: Intense secondary aerosol formation due to strong atmospheric photochemical reactions in summer: observations at a rural site in eastern Yangtze River Delta of China, The Science of the total environment, 571, 1454-1466, 10.1016/j.scitotenv.2016.06.212, 2016a.

Wang, H.L., Qiao, L.P., Lou S.R., Zhou, M., Ding, A.J., Huang, H.Y., Chen, J.M., Wang, Q., Tao, S.K., Chen, C.H., Li L., and Huang C.: Chemical composition of PM2.5 and meterological impact among three years in urban Shanghai, China, Journal of Cleaner Proeuction, 112, 2, 1302-1311, 2016b.

Wang, H., Lu, K., Chen, X., Zhu, Q., Chen, Q., Guo, S., Jiang, M., Li, X., Shang, D., Tan, Z., Wu, Y., Wu, Z., Zou, Q., Zheng, Y., Zeng, L., Zhu, T., Hu, M., and Zhang, Y.: High N2O5 Concentrations Observed in Urban Beijing: Implications of a Large Nitrate Formation Pathway, Environmental Science & Technology Letters, 4, 416-420, 10.1021/acs.estlett.7b00341, 2017.

Wang, J., Ge, X., Chen, Y., Shen, Y., Zhang, Q., Sun, Y., Xu, J., Ge, S., Yu, H., and Chen, M.: Highly time-resolved urban aerosol characteristics during springtime in Yangtze River Delta, China: insights from soot particle aerosol mass spectrometry, Atmospheric Chemistry and Physics, 16, 9109-9127, 10.5194/acp-16-9109-2016, 2016c.

Wang, J., Zhao, B., Wang, S., Yang, F., Xing, J., Morawska, L., Ding, A., Kulmala, M., Kerminen, V.-M., Kujansuu, J., Wang, Z., Ding, D., Zhang, X., Wang, H., Tian, M., Petäjä, T., Jiang, J., Hao, J., Particulate matter pollution over China and the effects of control policies, Science of the Total Environment, 584, 426-447, 2017a.

Wang, T., Nie, W., Gao, J., Xue, L. K., Gao, X. M., Wang, X. F., Qiu, J., Poon, C. N., Meinardi, S., Blake, D., Wang, S. L., Ding, A. J., Chai, F. H., Zhang, Q. Z., and Wang, W. X.: Air quality during the 2008 Beijing Olympics: secondary pollutants and regional impact, Atmospheric Chemistry and Physics, 10, 7603-7615, 2010.

Wang, T., Tham, Y. J., Xue, L. K., Li, Q. Y., Zha, Q. Z., Wang, Z., Poon, S. C. N., Dube, W. P., Blake, D. R., Louie, P. K. K., Luk, C. W. Y., Tsui, W., and Brown, S. S.: Observations of nitryl chloride and modeling its source and effect on ozone in the planetary boundary layer of southern China, J Geophys Res-Atmos, 121, 2476-2489, 10.1002/2015JD024556, 2016d.

Wang, X., and Zhang, Y.: Particulate Nitrate Formation in a Highly Polluted Urban Area: A Case Study by Single-Particle Mass Spectrometry in Shanghai Environ. Sci. Technol, 43, 3061-3066, 2009.

Wang, X., Ding, X., Fu, X., He, Q., Wang, S., Bernard, F., Zhao, X., and Wu, D.: Aerosol scattering coefficients and major chemical compositions of fine particles observed at a rural site in the central Pearl River Delta, South China, Journal of Environmental Sciences, 24, 72-77, 10.1016/s1001-0742(11)60730-4, 2012.

Wang, X. F., Chen, J. M., Sun, J. F., Li, W. J., Yang, L. X., Wen, L., Wang, W. X., Wang, X. M., Collett, J. L., Shi, Y., Zhang, Q. Z., Hu, J. T., Yao, L., Zhu, Y. H., Sui, X., Sun, X. M., and Mellouki, A.: Severe haze episodes and seriously polluted fog water in Ji'nan, China, Sci Total Environ, 493, 133-137, 2014.

Wang, X., Wang, H., Xue, L., Wang, T., Wang, L., Gu, R., Wang, W., Tham, Y. J., Wang, Z., Yang, L., Chen, J., and Wang, W.: Observations of N_2O_5 and $ClNO_2$ at a polluted urban surface site in North China: High N_2O_5 uptake coefficients and low $ClNO_2$ product yields, Atmospheric Environment, 156, 125-134, 10.1016/j.atmosenv.2017.02.035, 2017b.

Wen, L., Chen, J., Yang, L., Wang, X., Caihong, X., Sui, X., Yao, L., Zhu, Y., Zhang, J., Zhu, T., and Wang, W.: Enhanced formation of fine particulate nitrate at a rural site on the North China Plain in summer: The important roles of ammonia and ozone, Atmospheric Environment, 101, 294-302, 10.1016/j.atmosenv.2014.11.037, 2015.

Wen, L., Xue, L., Wang, X., Xu, C., Chen, T., Yang, L., Wang, T., Zhang, Q., and Wang, W.: Summertime fine particulate nitrate pollution in the North China Plain: increasing trends, formation mechanisms and implications for control policy, Atmospheric Chemistry and Physics, 18, 11261-11275, 10.5194/acp-18-11261-2018, 2018.

Xie, Y., Ding, A., and Nie, W.: Enhanced sulfate formation by nitrogen dioxide: Implications from in situ observations at the SORPES station Journal Of Geophysical Research: Atmospheres, 120, 12,679-612,964, 10.1002/, 2015.

Xue., J., and Yuan., Z.: Insights into factors afferting nitrate in PM2.5 in a polluted high NOx environment through hourly observations and size distribution measurements Journal of Geophysical Research: Atmospheres, 119, 4888-4902, 10.1002/, 2013.

Yang, T., Sun, Y., Zhang, W., Wang, Z., Liu, X., Fu, P., and Wang, X.: Evolutionary processes and sources of high-nitrate haze episodes over Beijing, Spring, J Environ Sci (China), 54, 142-151, 10.1016/j.jes.2016.04.024, 2017.

Young, D. E., Kim, H., Parworth, C., Zhou, S., Zhang, X., Cappa, C. D., Seco, R., Kim, S., and Zhang, Q.: Influences of emission sources and meteorology on aerosol chemistry in a polluted urban environment: results from DISCOVER-AQ California, Atmospheric Chemistry and Physics, 16, 5427-5451, 10.5194/acp-16-5427-2016, 2016.

Zhang, Q., Canagaratna, M. R., Jayne, J. T., Worsnop, D. R., and Jimenez, J. L.: Time- and size-resolved chemical composition of submicron particles in Pittsburgh: Implications for aerosol sources and

695   processes, J Geophys Res-Atmos, 110, 2005.

696 Zhang, Y., Tang, L., Yu, H., Wang, Z., Sun, Y., Qin, W., Chen, W., Chen, C., Ding, A., Wu, J., Ge, S.,
697   Chen, C., and Zhou, H.-c.: Chemical composition, sources and evolution processes of aerosol at an
698   urban site in Yangtze River Delta, China during wintertime, Atmospheric Environment, 123, 339-
699   349, 10.1016/j.atmosenv.2015.08.017, 2015a.

700 Zhang, Y. J., Tang, L. L., Wang, Z., Yu, H. X., Sun, Y. L., Liu, D., Qin, W., Canonaco, F., Prévôt, A. S.
701   H., Zhang, H. L., and Zhou, H. C.: Insights into characteristics, sources, and evolution of submicron
702   aerosols during harvest seasons in the Yangtze River delta region, China, Atmospheric Chemistry
703   and Physics, 15, 1331-1349, 10.5194/acp-15-1331-2015, 2015b.

704 Zhang, Y. W., Zhang, X. Y., Zhang, Y. M., Shen, X. J., Sun, J. Y., Ma, Q. L., Yu, X. M., Zhu, J. L., Zhang,
705   L., and Che, H. C.: Significant concentration changes of chemical components of PM1 in the
706   Yangtze River Delta area of China and the implications for the formation mechanism of heavy haze-
707   fog pollution, The Science of the total environment, 538, 7-15, 10.1016/j.scitotenv.2015.06.104,
708   2015c.

709 Zhang, Y., Ding, A., Mao, H., Nie, W., Zhou, D., Liu, L., Huang, X., and Fu, C.: Impact of synoptic
710   weather patterns and inter-decadal climate variability on air quality in the North China Plain during
711   1980-2013, Atmos. Environ., 124, 119-128, 2016.

712 Zou, J., Liu, Z., Hu, B., Huang, X., Wen, T., Ji, D., Liu, J., Yang, Y., Yao, Q., and Wang, Y.: Aerosol
713   chemical compositions in the North China Plain and the impact on the visibility in Beijing and
714   Tianjin, Atmospheric Research, 201, 235-246, 10.1016/j.atmosres.2017.09.014, 2018.
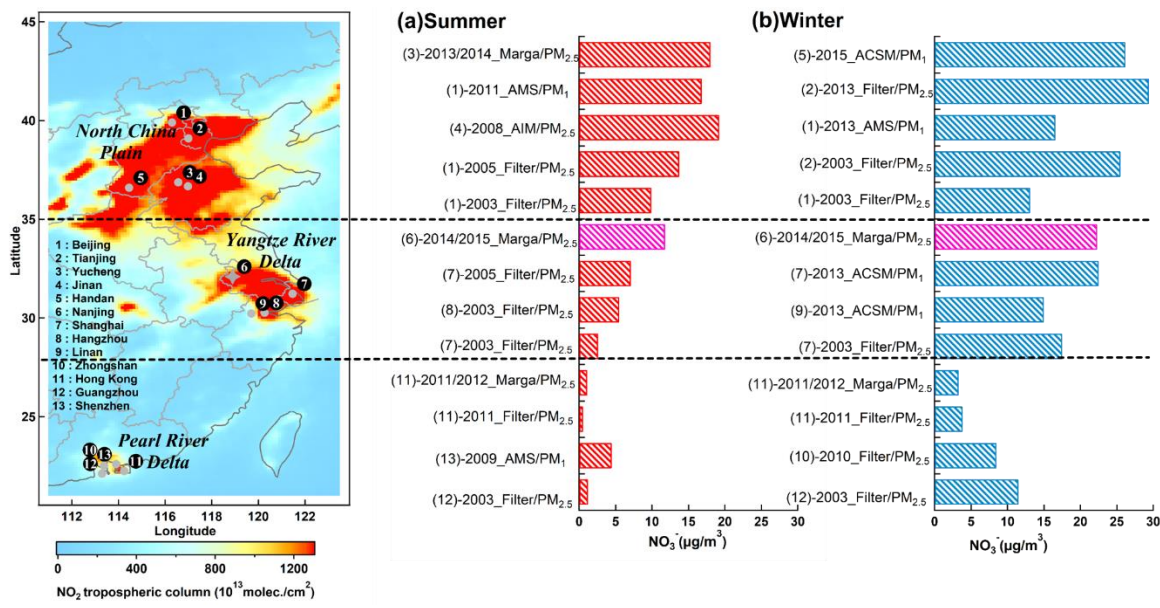
Figure 1 Average mass concentrations of particulate nitrate at different sampling sites in **(a)** summer and **(b)** winter. The left panel shows the map color-coded by 2-years (2014-2015) averaged tropospheric NO_2 from OMI satellite (http://www.temis.nl/airpollution/no2.html). The pink bars are for this study.
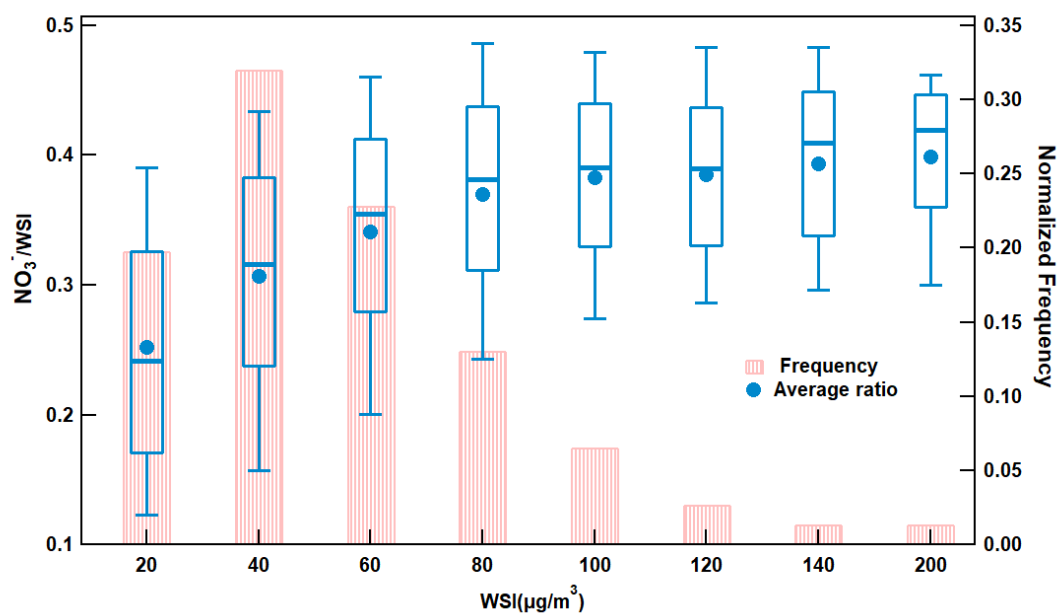
Figure 2 Average proportion of nitrate and normalized frequency of occurrence at different mass concentration bins of water soluble ions at SORPES. For the ratio, box boundaries represent the interquartile range, bars represent 5%-95% percentile range, and horizontal lines represent the median value.
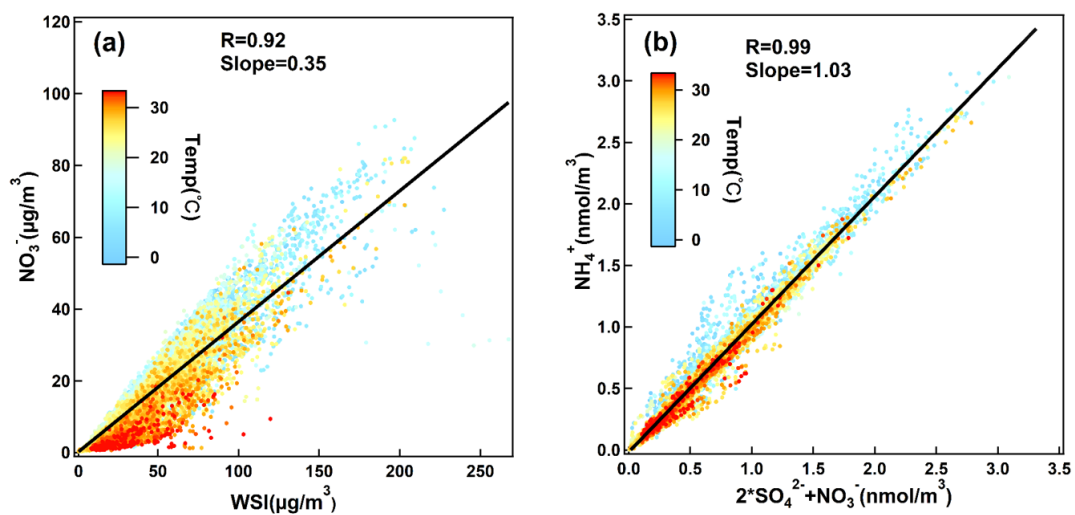
Figure 3 Scatter plots of **(a)** nitrate vs. total WSI color coded by air temperature, **(b)** molar concentrations of ammonium with nitrate molar concentrations plus two times of sulfate molar concentrations.
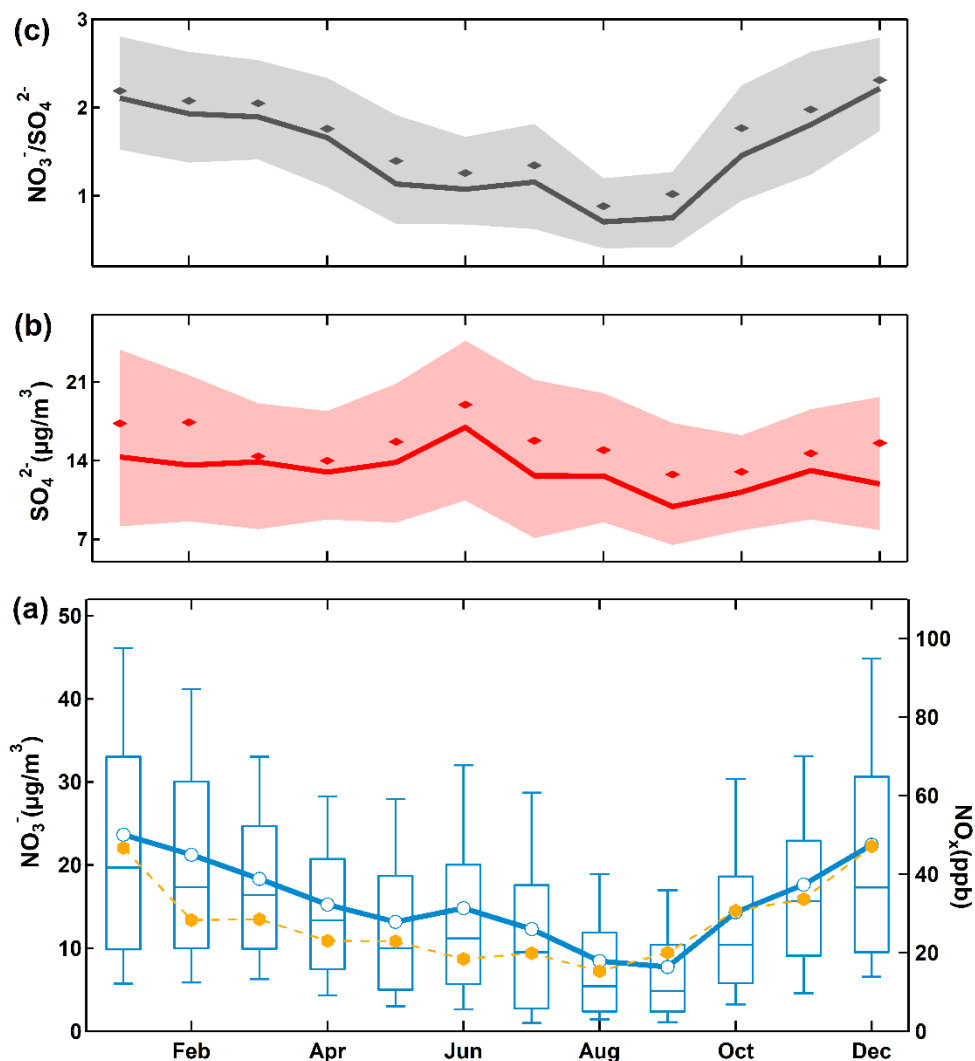
Figure 4 Monthly averaged nitrate (blue), sulfate (red), NO_x (orange) mass concentrations and nitrate to sulfate molar-based ratio (grey) measured at SORPES station during March 2014 to February 2016. For nitrate to sulfate ratio (a) and sulfate (b), bold solid lines are the median values, shade areas represent percentiles of 75% and 25%, and diamonds represent the mean values. For nitrate (c), box boundaries represent the interquartile range, bars represent 5%-95% percentile range, horizontal lines represent the median value, and crosses represent mean values.
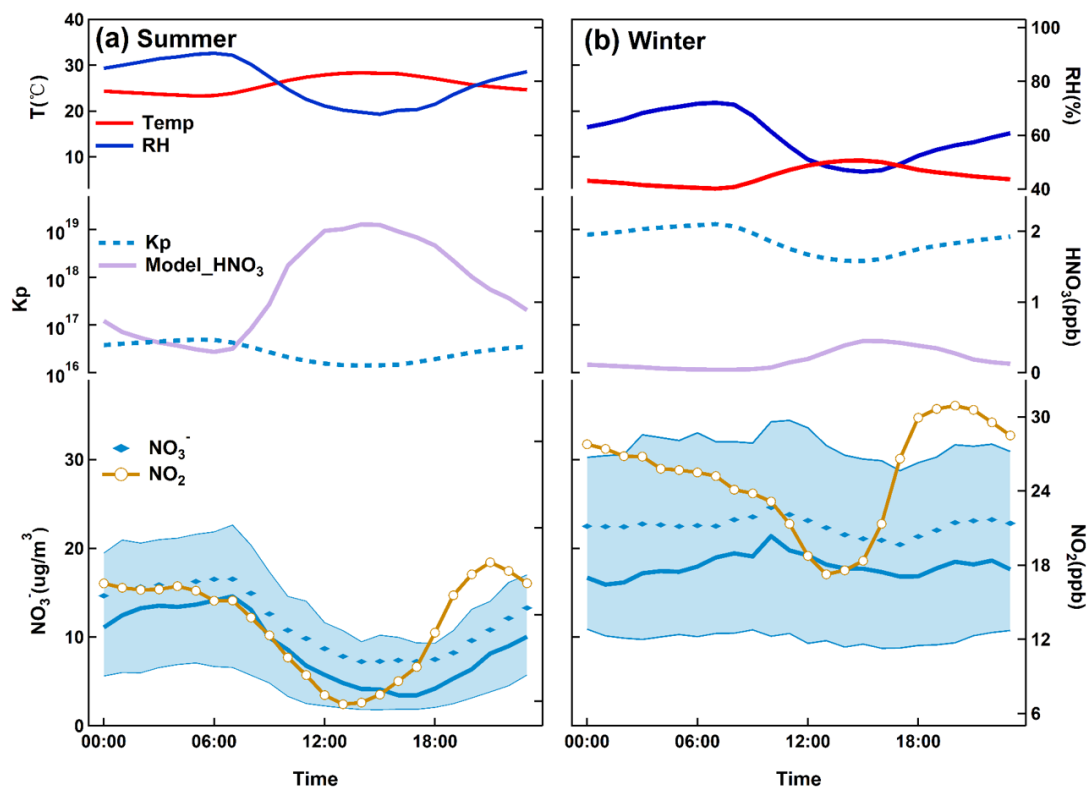
Figure 5 Diurnal variation of particulate nitrate in **(a)** summer and **(b)** winter. For nitrate, bold solid lines are the median values, shaded areas represent percentiles of 75% and 25% and diamonds represent mean values. Diurnal averages of NO_2 and modeled nitric acid mass concentrations are also provided with temperature and RH.
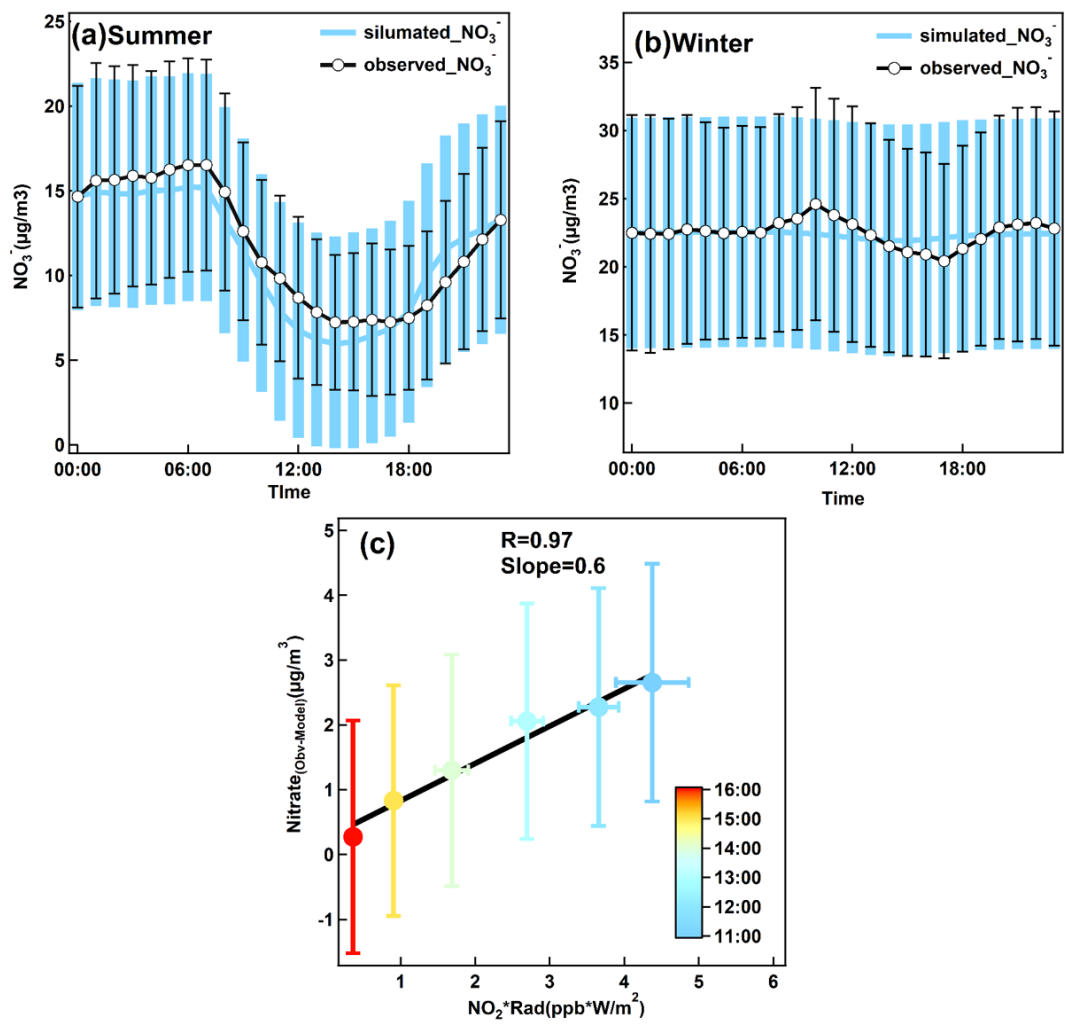
Figure 6 Modeled nitrate diurnal variations in **(a)** summer and **(b)** winter, together with the observed nitrate concentrations. Error bars provided are the standard deviation of the mean at each hourly interval. **(c)** Scatter plot of the difference between model and observed nitrate average mass concentrations with the product of NO_2 and radiation color coded by the hour of day for the samples.
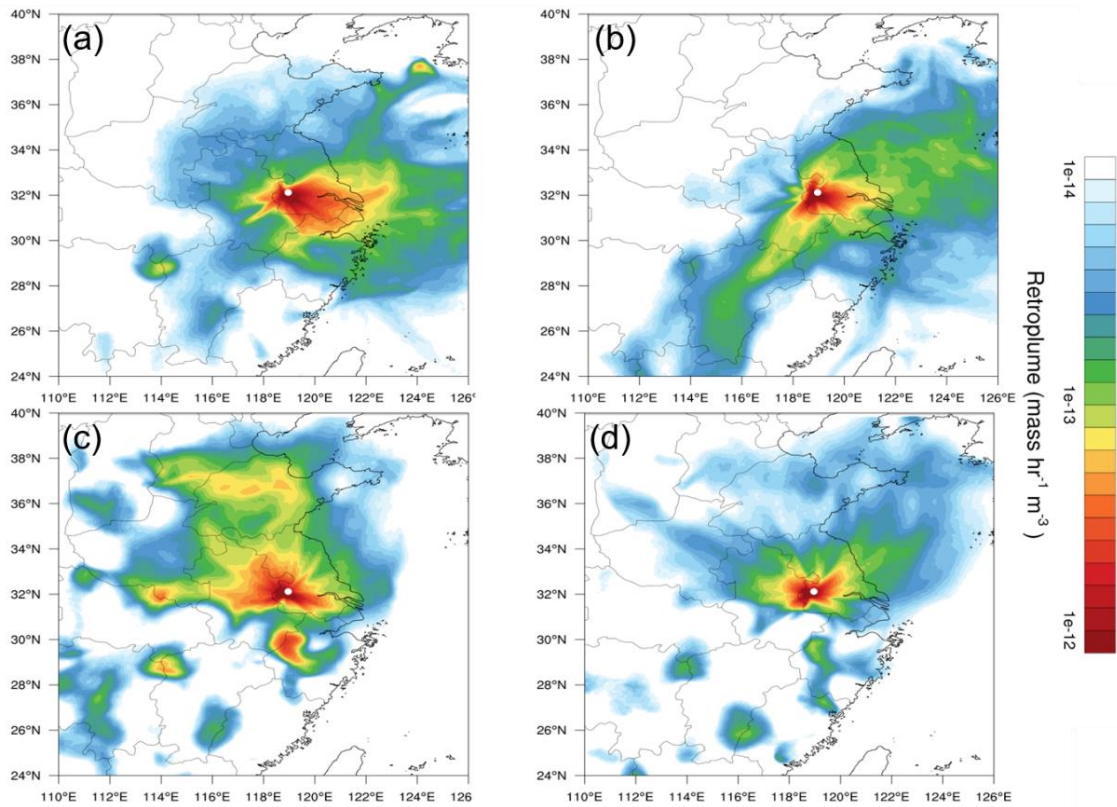
Figure 7 The averaged retroplumes (i.e., 100 m footprint) of the selected events: **(a)** Top 25% nitrate concentrations in summer, **(b)** Bottom 25% nitrate concentrations in summer, **(c)** Top 25% nitrate concentrations in winter, and **(d)** Bottom 25% nitrate concentrations in winter.
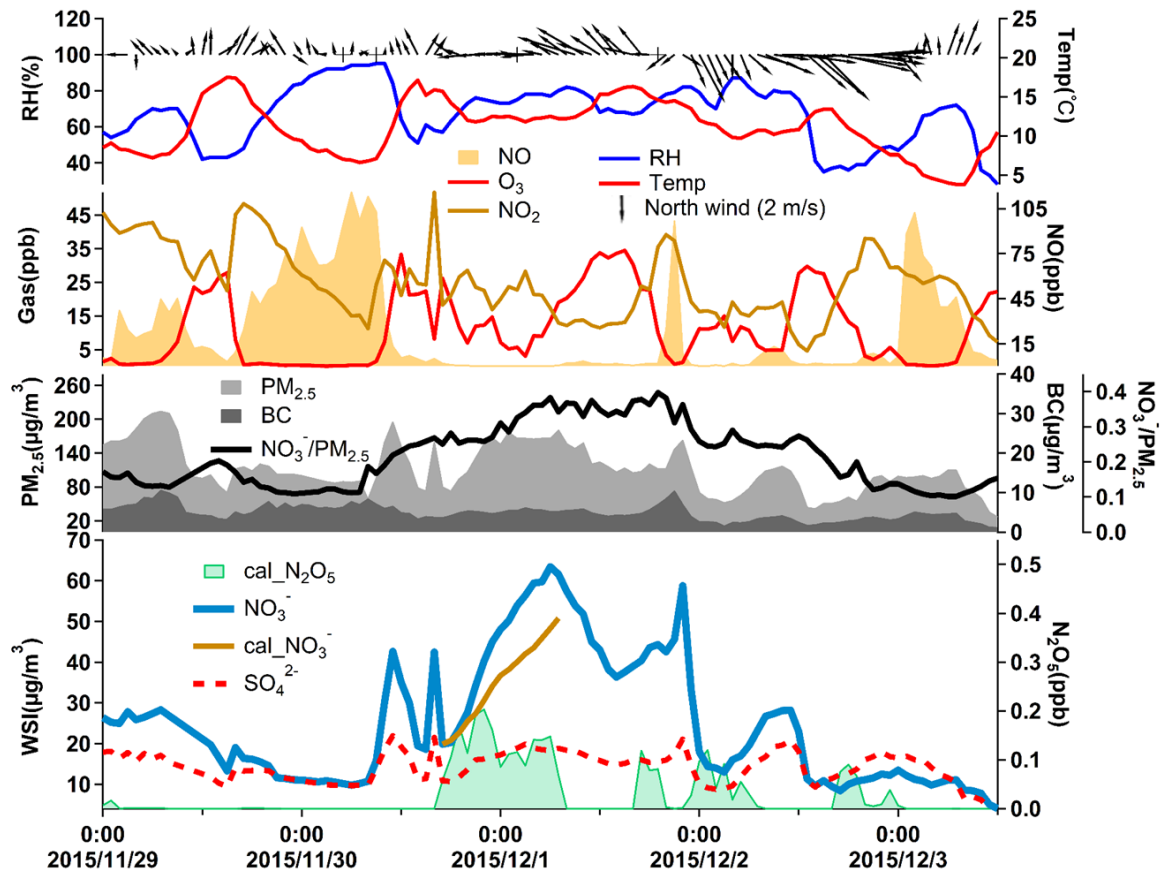
Figure 8 Time series of meteorological data and the concentrations of trace gases related to nitrate formation during 29 November to 3 December, 2015. Cal_NO_3^- represents the nitrate concentrations calculated from the hydrolysis of N_2O_5.
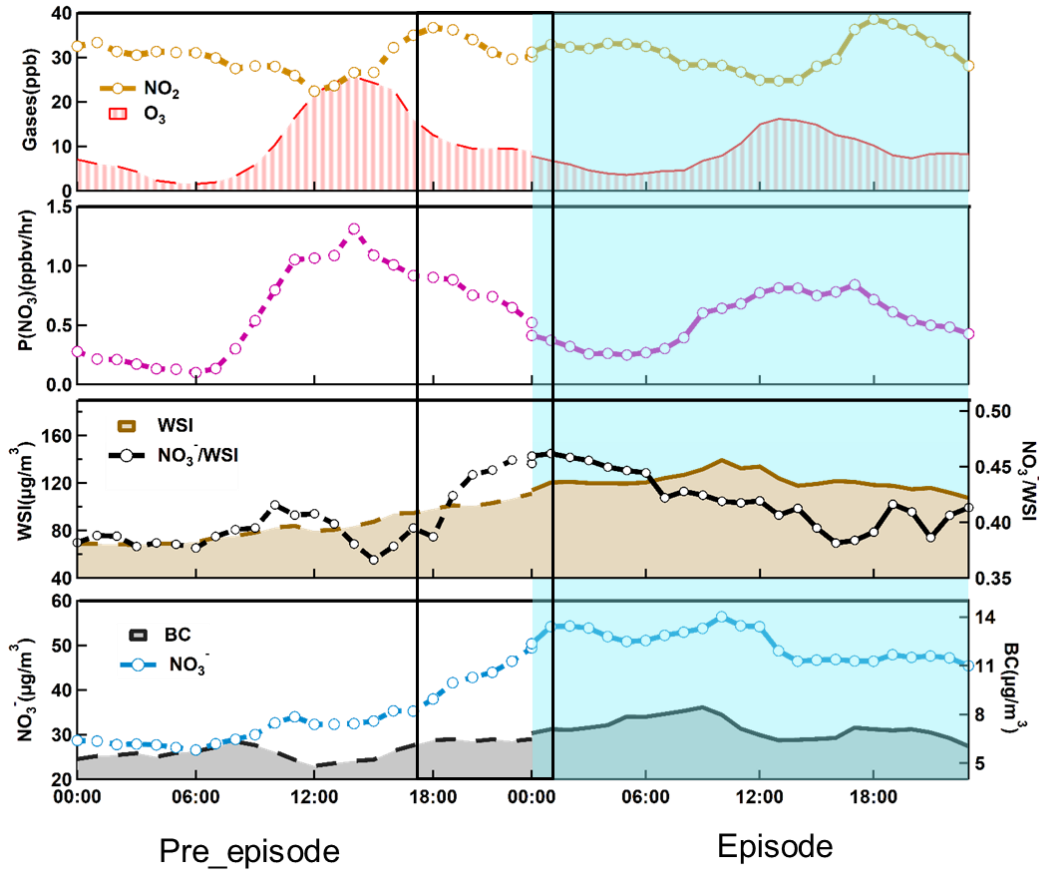
Figure 9 Diurnal variations of particulate nitrate, black carbon, the total water soluble ions, nitrate to WSI ratio, P (NO$_3$), NO$_2$, and O$_3$ averaged for nitrate episode days with exceedances of one mean plus two standard deviations. The left side shows the pre-episode days and the right side shows the episode days during the winter of entire two years period. The solid line box corresponds to the rapid growth of nitrate at night. It should be noted that P(NO$_3$) is calculated by the product of NO$_2$ and O$_3$ multiplied by the rate constant k$_1$ of NO$_2$+O$_3$ reaction.
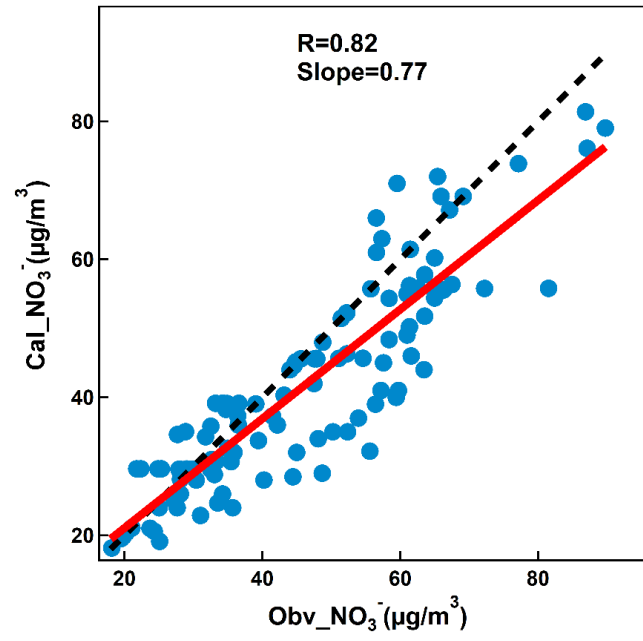
Figure 10 Scatter plot of calculated nitrate concentrations and observed nitrate concentrations from 17:00 to 23:00 of each episode.

Table 1 major gas phase and heterogeneous reactions involved NO_3 and N_2O_5

Reaction	Rate constant
$NO_2+O_3\rightarrow NO_3+O_2$	$k_1=1.28\times10^{13}\times EXP(-2470/T)$
$NO_3+NO_2\leftrightarrow N_2O_5$	$k_{eq}=1.73\times10^{-13}\times EXP(1550/T)$
$NO_3+NO\leftrightarrow NO_2+NO_2$	$k_3=1.8\times10^{-11}\times EXP(110/T)$
$NO_3\rightarrow NO+O_2$	j_4
$NO_3\rightarrow NO+O_2$	j_5
$NO_3 \xrightarrow{voc} products$	$k_6=\sum(k_{voci}\cdot[voc]_i)$
$NO_3 \xrightarrow{Heterogeneous} products$	$k_7=0.25\cdot i\cdot C_{NO_3}\cdot\gamma_{NO_3}\cdot S_{aerosol}$
$N_2O_5 \xrightarrow{Heterogeneous} products$	$k_8=0.25\cdot C_{N_2O_5}\cdot\gamma_{N_2O_5}\cdot S_{aerosol}$